AGU PUBLICATIONS

JGR

Journal of Geophysical Research: Earth Surface

RESEARCH ARTICLE
10.1002/2014JF003403

Key Points:
- Climate controls explaining strath terrace formation are not process specific
- Hillslope sediment flux alone may be insufficient to create strath terraces
- Punctuated bedrock incision can occur during periods of channel aggradation

Correspondence to:
A. L. Langston,
abigail.langston@colorado.edu

Citation:
Langston, A. L., G. E. Tucker, and R. S. Anderson (2015), Interpreting climate-modulated processes of terrace development along the Colorado Front Range using a landscape evolution model, *J. Geophys. Res. Earth Surf.*, *120*, 2121–2138, doi:10.1002/2014JF003403.

Received 5 DEC 2014
Accepted 21 SEP 2015
Accepted article online 24 SEP 2015
Published online 20 OCT 2015

Interpreting climate-modulated processes of terrace development along the Colorado Front Range using a landscape evolution model

Abigail L. Langston[1], Gregory E. Tucker[1], and Robert S. Anderson[2]

[1]Cooperative Institute for Research in Environmental Sciences and Department of Geological Sciences, University of Colorado Boulder, Boulder, Colorado, USA, [2]Institute of Arctic and Alpine Research and Department of Geological Sciences, University of Colorado Boulder, Boulder, Colorado, USA

Abstract Flights of terraces that flank range fronts throughout the Rocky Mountains record episodic stream incision over the past 1.5 Ma. Studies dating terraces in the Denver Basin along the Colorado Front Range suggest that these high surfaces were formed during glacial intervals and were rapidly incised and abandoned during interglacials. Modulation of sediment supply or transport capacity associated with climate change related to glacial-interglacial cycles have been suggested as possible drivers for the repeated aggradation and abandonment of these high surfaces. Potential mechanisms for increasing sediment supply and transport in rivers include variations over time in sediment flux from intermittently glaciated major valleys, the efficiency of hillslope sediment transport, and the magnitude and timing of rainfall intensity and stream flow. In this study, we use a landscape evolution model to determine whether any of these processes, in isolation or in combination, is sufficient to explain the observed rates and patterns of terrace formation and abandonment along the Colorado piedmont. Cycles of channel aggradation and incision are apparent in the models when either mean rainfall intensity is varied or a glacial source of sediment is added. The models suggest that in the absence of a large addition of sediment to the streams, changes in stream power are necessary to allow channel aggradation and the planation of bedrock surfaces, and increased sediment flux from hillslopes is necessary to match observations of increased denudation rates that coincide with the deposition of terrace-capping gravels.

1. Introduction

Strath terraces record the incision history of rivers in response to variations in base level or climate. The mechanisms through which tectonic uplift can trigger incision of strath terrace surfaces are well understood [e.g., *Merritts et al.*, 1994]. Climatically influenced changes in sediment supply and carrying capacity have been linked to terrace development in many studies [*Meyer et al.*, 1995; *Wegmann and Pazzaglia*, 2002; *Vandenberghe*, 2003], but it is unclear how specific climate processes, such as changes in sediment supply, rainfall intensity, and peak discharge, drive strath terrace formation and how strong these climate forcings must be in order for strath terraces to develop.

Strath terraces are formed by lateral planation of a bedrock surface by a river, followed by rapid vertical incision, leading to abandonment of this surface that is often capped with fluvial sediment. In order to develop strath terraces, the ratio of lateral bedrock planation to vertical incision must change through time [*Gilbert*, 1877; *Merritts et al.*, 1994; *Hancock and Anderson*, 2002]. Periods of lateral planation occur in a graded or an aggrading river when sediment blanketing the bed of the river protects the bed from vertical incision, and erosion is focused toward the sides of the channel [*Bull*, 1990; *Hancock and Anderson*, 2002; *Johnson and Whipple*, 2010]. A transition from lateral bedrock beveling to vertical incision can occur when sediment supply decreases or stream discharge increases. When the carrying capacity of the stream exceeds the sediment load, sediment on the bed of the stream is stripped, allowing renewed vertical incision into the bedrock and abandonment of the strath terrace. Lateral bedrock erosion and strath terrace development occur more readily in soft bedrock, such as shale or weakly indurated sandstone [*Montgomery*, 2004; *Brocard and Van der Beek*, 2006]. Channels in soft bedrock (and especially those with headwaters in harder bedrock) may be more likely to be protected from vertical incision by a blanket of sediment, allowing lateral erosion of channel walls but inhibiting vertical incision [*Brocard and Van der Beek*, 2006].

A number of processes have been invoked to explain the shifts between lateral erosion and vertical incision that develop strath terraces. These include terrace abandonment due to meander cutoffs [*Finnegan and Dietrich*, 2011], transition from a single thread stream to a braided stream [*Finnegan and Balco*, 2013], increased sediment load from glacial sources [*Hancock and Anderson*, 2002; *Brocard et al.*, 2003], increased sediment supply from intensified hillslope processes [*Wegmann and Pazzaglia*, 2002], increased stream power from changes in rainfall intensity [*Hanson et al.*, 2006], and a combination of both changes in sediment flux and transport capacity [*Pierce et al.*, 2011]. Although the relationship between stream power and sediment supply and likely periods of strath planation has been studied for some time [*Bull*, 1979], we do not fully understand the sensitivity of climate-induced changes in sediment load versus stream power. Different studies often invoke the same climate forcing mechanism and predict opposite results. For example, it is difficult to judge on the basis of intuition alone whether an increase in precipitation should produce incision due to increased hydraulic power or aggradation because of increased sediment yield from headwaters [*Tucker and Slingerland*, 1997].

The formation of strath terraces around the world has been tied to Pleistocene shifts between glacial and interglacial climate regimes, but various authors find that terraces form at the peak of glaciation [*Molnar et al.*, 1994; *Hancock et al.*, 1999], at the transition from a glacial to an interglacial climate [*Pan et al.*, 2003], or during interglacial intervals [*DeVecchio et al.*, 2012]. The widely varying ages of strath terrace formation can be attributed to the proximity of the terraces to glaciers and the different processes that influence sediment supply to streams in glaciated areas and unglaciated areas that feel the effects of climate shifts [*Church and Slaymaker*, 1989]. An additional concern in resolving the date of terrace abandonment is that in many studies there can be uncertainty in the ages of both the glacial maximum and the rapidly following deglaciation [e.g., *Molnar et al.*, 1994; *Hancock et al.*, 1999; *DeVecchio et al.*, 2012].

Few studies have modeled climate processes that result in strath terrace development in one-dimensional models [*Hancock and Anderson*, 2002]. *Hancock and Anderson* [2002] found that changing the inputs of sediment load and water discharge allows the stream to shift from primarily eroding laterally, to incising vertically, resulting in flights of strath terraces. *Finnegan and Dietrich* [2011] proposed that flights of strath terraces can develop independently from variations in climate or tectonic uplift through meander cutoffs that incite knickpoint migration, vertical incision, and abandonment of the terrace surface. These previous modeling efforts laid a foundation for determining the mechanisms that drive terrace planation and abandonment, but did not address the basinwide contribution of water and sediment to terrace genesis. In this study, we use a two-dimensional landscape evolution model to determine whether climate-driven changes in sediment flux from a glacier, sediment flux from hillslopes, or mean rainfall intensity, either in isolation or in combination, are sufficient to explain observed rates and patterns of strath terrace formation and abandonment. This is the first use of a two-dimensional landscape evolution model to explore formation of strath terraces at the edge of a mountain range. We are able to address the relative impact of each of these climate drivers on cyclic channel aggradation and incision, as well as lateral movement and valley widening of the channel.

1.1. Field Area

Flights of strath terraces flank the streams that drain the Colorado Front Range (Figure 1), recording periodic episodes of lateral bedrock erosion that results in a broad surface capped by fluvial gravel, followed by vertical incision of bedrock and terrace abandonment. The terraces are located at the transition from the rugged mountain core to the adjacent High Plains. The mountains of the Front Range consist of a resistant core of Paleoproterozoic-aged granitic and metamorphic rocks, while the High Plains are underlain by easily eroded Cretaceous-aged Pierre shale and poorly lithified Tertiary sedimentary units. We focus on terraces formed by three streams that flow from the mountains onto the plains: Lefthand Creek, Boulder Creek, and Coal Creek (Figure 1). One of the unique characteristics of these terraces is that they are present in watersheds of varying size. Boulder Creek has a drainage area of 1158 km^2 and has many levels of terraces that range from 5 to >100 m above the current streams. Lefthand Creek and Coal Creek are smaller watersheds (145 km^2 and 91 km^2, respectively), and have flights of terraces, including very broad terraces (Table Mountain and Rocky Flats), in their watersheds. The headwaters of Boulder Creek were repeatedly glaciated during the late Pleistocene, but there is no evidence for significant past glaciation within the current watershed boundaries for either Lefthand Creek or Coal Creek [*Madole et al.*, 1998] (Figure 1).

The terraces are capped with fluvial sand and gravel that were deposited either simultaneously with the beveling of the bedrock surface or after the initial strath carving, during a period of river occupation of the surface.

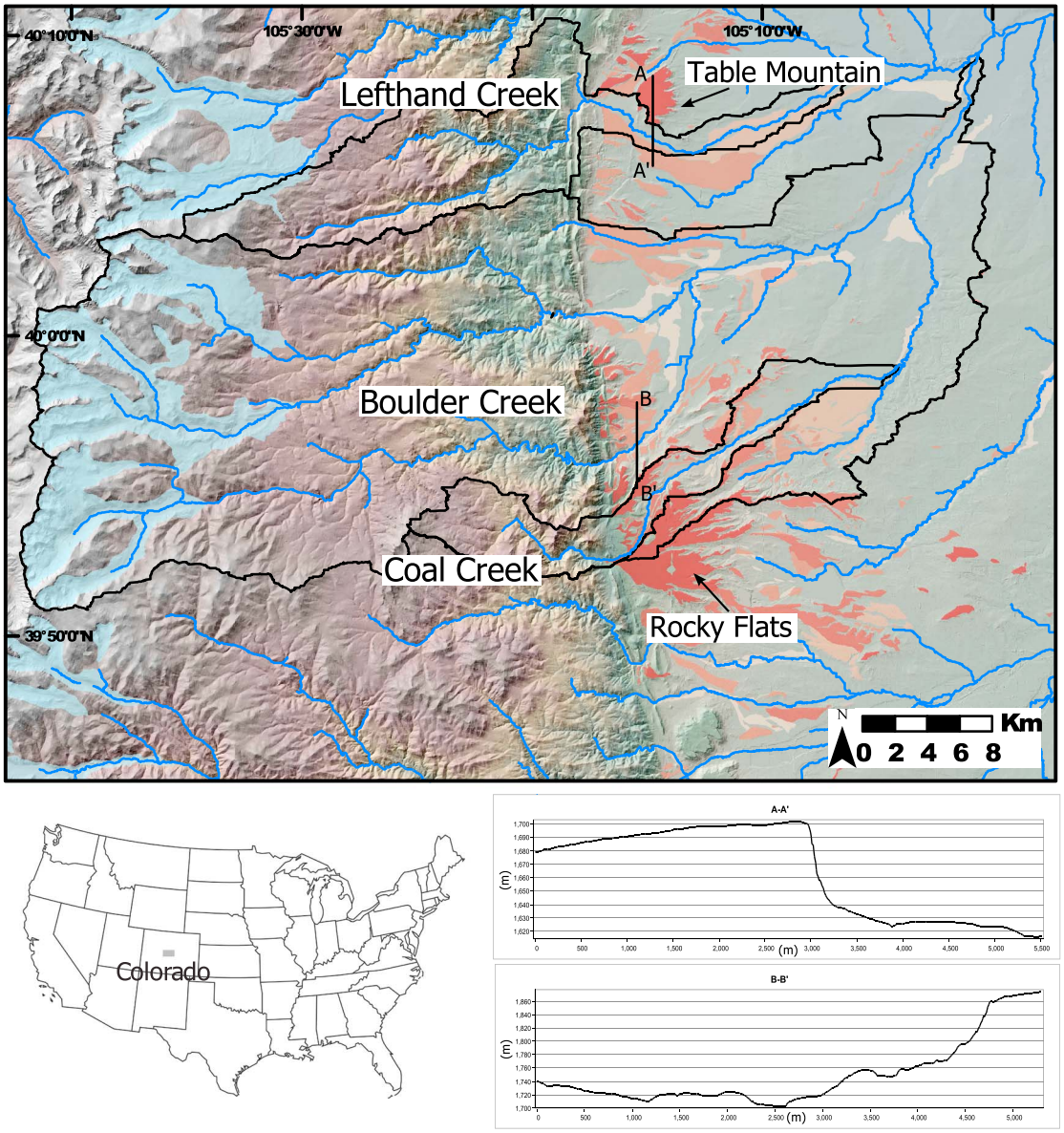

Figure 1. Hillshade image showing the three focus watersheds in the study area of the Denver Basin. The streams undergo an abrupt transition from the rugged, high-relief mountains to the low-relief plains. Light green shading in the high alpine reaches shows the glacial extent at the last glacial maximum [*Madole et al.*, 1998]. Terraces on the low relief plains are colored according to their height above modern stream level, with darker colors indicating highest terraces and lighter colors indicating lowest terraces. Cross-section A-A' shows elevation of Table Mountain ~75 m above Lefthand Creek. Cross-section B-B' shows elevation of terraces flanking South Boulder Creek that are 40 to >100 m above South Boulder Creek.

The sediments capping Table Mountain are 5–10 m thick and are composed of coarse-grained material, up to 30 cm in diameter, in a matrix of fine sediment. The coarse fraction consists of granite, granodiorite, sandstone, and metamorphic rocks, reflecting sourcing of this material from throughout the Lefthand Creek catchment [*Dühnforth et al.*, 2012]. The sediment cap on the Rocky Flats surface consists of 5–10 m of fluvial gravel and interbedded sand with a grain size distribution similar to that of Table Mountain [*Riihimaki et al.*, 2006]. The older terraces are atypical of fluvial straths because they are unusually broad, and in the case of Rocky Flats, appear to bury an undulating bedrock surface that contains evidence of multiple paleochannels [*Knepper*, 2005], rather than a smooth bedrock surface.

Studies dating the abandonment of several terrace surfaces suggest that rivers occupied the surfaces and cut laterally for long periods during glacial intervals and rapidly incised vertically during interglacial intervals. *Riihimaki et al.* [2006] used in situ ^{10}Be and ^{26}Al to date two sites from the alluvium capping the Rocky Flats

surface, which is ~100 m higher than local base level (Figure 1, B-B′ transect). The ages of the sites range from 380 kyr to 780 kyr. Vertical profiles in the Rocky Flats surface show a complex fluvial history of deposition, incision, and redeposition and suggest that the Rocky Flats surface was occupied for hundreds of thousands of years from 2.4 Ma.

Dühnforth et al. [2012] used both in situ and meteoric ^{10}Be to date the abandonment of several terraces, including Table Mountain, which is also ~100 m higher than local base level (Figure 1, A-A′ transect). They found an abandonment age for Table Mountain of 95 kyr, which is younger by an order of magnitude than previously inferred from elevation relationships of the few dated terraces in the basin [*Madole*, 1991]. These young dates suggest that terrace treads were occupied and beveled for long periods before being abandoned following bursts of rapid incision, at rates of up to several mm/yr [*Dühnforth et al.*, 2012]. *Foster et al.* [2013] used ^{10}Be to date a lower elevation terrace near Table Mountain and report a preliminary abandonment age for the lower terrace that is close to the abandonment age of 95 kyr for Table Mountain reported by *Dühnforth et al.* [2012]. *Foster et al.* [2013] also calculated paleodenudation rates from cosmogenic radionuclide inheritance in the sediments capping Table Mountain. They report a basin-averaged paleodenudation rate during the deposition of the Table Mountain terrace sediments that is up to 2–3 times higher than the modern denudation rate of 0.25 mm/yr [*Dethier and Lazarus*, 2006].

Schildgen et al. [2002] found the youngest absolute ages of any terraces dated in the study area. They dated fill terraces within Boulder Canyon at >100 kyr (15–20 m above channel), 32–10 kyr (4–15 m above the channel), and Holocene age (<4 m above the channel) and argued for net excavation of sediment during transitions from glacial to interglacial intervals. They interpreted the decline in the height of the terraces as evidence for rapidly changing stream load and/or stream power.

2. Methods and Model Setup

We use the CHILD landscape evolution model [*Tucker et al.*, 2001] to construct a scaled model landscape that includes the sharp transition from the high-relief Front Range to the low-relief High Plains (Figure 2). The relief of the mountains in the model is created by assigning low bedrock erodibility ($K_b = 2.5 \times 10^{-4}$ kg/yr^2 m) and by dictating that regolith produced in the mountains is 90% coarse-grained material (5 cm in diameter) and 10% fine-grained material (1 mm in diameter). The adjacent plains are assigned a much higher bedrock erodibility ($K_b = 1$ kg/yr^2 m), and regolith produced on the plains is 90% fine-grained material and 10% coarse-grained material (Figure 2). These parameters serve to represent the strong granodiorite core of the Front Range and the weak, friable shale bedrock of the High Plains. Long-term lowering of regional base level is represented by applying a steady, uniform rate of vertical motion (0.1 mm/yr) to the interior model nodes, while leaving the bottom boundary fixed at zero elevation. This configuration means that the model runs in the frame of reference of a steadily eroding surface (Figure 2).

The model measures 800 m by 1600 m with 20 m cell spacing. This downscaling was required for computational efficiency at the necessary cell resolution. In order to model the effect of hillslope processes on sediment supply to the rivers of the Front Range, the cell size in the model needs to be no larger than about 20 m. The model is intended to represent a hypothetical catchment at the skirts of a crystalline mountain range, rather than entirely recreating the watersheds that drain the Front Range. One possible consequence of focusing on such a small scale is that the model is likely to underpredict the scale of fluvial incision and aggradation that occurs in nature. For example, take a model where aggradation occurs over 800 m compared to a model where aggradation occurs over 8 km. If sedimentation causes the channel slope to increase by the same amount in both the small and the large models, the magnitude of aggradation will be 10 times larger in the larger model. Thus, direct comparison of model predictions to observations in nature must be made cautiously.

Regolith is produced from bedrock by weathering and erosion and redeposition of rock by fluvial processes. In the model, both diffusive creep and fluvial erosion are modeled in all cells; however, for the purposes of this study, we consider convex areas that erode primarily through diffusive creep to be the hillslopes and concave areas that are eroded primarily by fluvial processes to be the channels. The fluvial erosion component only allows vertical incision and aggradation; there is no mechanism that allows the channel to erode laterally.

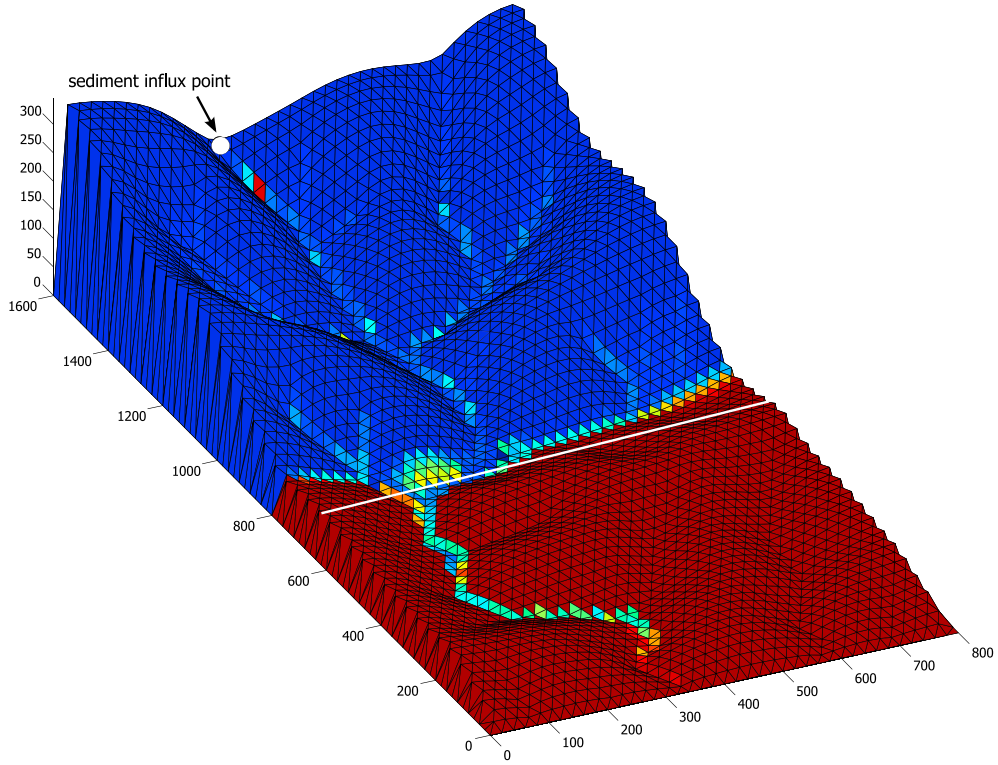

Figure 2. Model domain representing a scaled-down version of the crystalline core of the Front Range (high-relief area, y > 800 m) and the low-relief High Plains (low-relief area, y < 800 m). The color overlay shows grain size distribution, with warm colors representing a high percentage of fine-grained material and the cool colors representing coarse-grained material. The coarse material is sourced from the mountains and has been spread on to the plains by the river as it moved across the plains. The river carries coarse sediment out of the mountains, and sediment in the stream fines as the river moves farther away from the mountains. Location of sediment influx point for the glacial sediment model is indicated by the white circle, and location of cross sections is indicated by the white line.

Evolution of regolith thickness, h, is described by the following mass conservation equation:

$$\frac{\partial h}{\partial t} = P_0 e^{-h/h_*} + K_d \nabla^2 \eta - \nabla q_c \tag{1}$$

where h is regolith thickness, P_0 is the maximum regolith production rate, h_* is a scaling depth, K_d is hillslope diffusivity, η is the land surface elevation, and ∇q_c is excess transport capacity of running water. The first term on the right describes production of regolith from bedrock weathering, which assumes that bedrock weathers isovolumetrically to regolith [*Heimsath et al.*, 1997]. The second term describes the diffusion of regolith downslope, which moves as a function of hillslope curvatures and K_d, a coefficient that describes the efficiency of the downslope movement [e.g., *Tucker and Hancock*, 2010]. The third term describes the transport of regolith by fluvial processes.

Land surface elevation is described by

$$\frac{\partial \eta}{\partial t} = U + K_d \nabla^2 \eta - F \tag{2}$$

where U is vertical motion relative to a given base level, and F is a fluvial erosion function.

The fluvial erosion function represents erosion rates from running water for both a transport-limited case and a detachment-limited case:

$$\begin{aligned} F &= \nabla q_c \text{ where } \quad D_c > \nabla q_c \\ F &= D_c \text{ elsewhere.} \end{aligned} \tag{3}$$

The detachment capacity of bedrock is calculated as a power law function of shear stress with a threshold term [*Tucker*, 2004]:

$$D_c = K_b(\tau^{3/2} - \tau_c^{3/2}) \tag{4}$$

where K_b is the bedrock erodibility coefficient, τ is the shear stress exerted on the bed, and τ_c is the critical shear stress needed to detach a given grain size [e.g., *Whipple et al.*, 2000].

The volumetric transport capacity of the flow for sand and gravel size fractions [L^3/T] is given by

$$\begin{aligned} Q_{cs} &= K_f W f_s \tau^{3/2}(1 - (\sqrt{\tau_{cs}/\tau}))^{4.5} \\ Q_{cg} &= K_f W f_g \tau^{3/2}(1 - (\tau_{cg}/\tau))^{4.5} \end{aligned} \tag{5}$$

where K_f is a transport efficiency factor, W is the width of the channel, f_s and f_g are the fractions of sand and gravel, and τ_{cs} and τ_{cg} are the critical shear stress for the entrainment of sand and gravel, respectively [*Gasparini et al.*, 1999].

The model represents terrain as an irregular grid of cells with surface water flow routed from cell to cell following the path of steepest descent [*Tucker et al.*, 2001]. The numerical approximation for excess transport capacity [L/T] in a cell i for a given grain size, j is as follows:

$$\nabla q_{cij} = \frac{Q_{cij} - \Sigma_{n=1}^{N} Q_{snj}}{\Lambda_i} \tag{6}$$

where Q_{cij} is the transport capacity of a given grain size j at cell i, Q_{snj} is the total fluvial sediment flux of grain size j from cell n to cell i, and Λ_i is the area of the cell. The summation is over N neighboring cells that contribute water and sediment directly to cell i. When ∇q_{ci} is negative, the stream does not have the capacity to carry its sediment load, and deposition occurs in a cell.

We use a stochastic storm generation model [*Tucker and Bras*, 2000] that iteratively draws storm intensity, storm duration, and interstorm duration from a Poisson distribution, given mean values of each. We initially set mean precipitation intensity to 10 m/yr (1.14 mm/h), storm duration to 0.1 year, and interstorm duration to 0.9 year. The mean storm duration 0.1 year, or 877 h, is about 2 orders of magnitude longer than typical storm lengths. In nature, individual storm events last on the order of minutes to hours [*Eagleson*, 1978], with some exceptional storms lasting days. The values for storm and interstorm duration used in the model (0.1 year and 0.9 year, respectively) capture the seasonal variability in climate seen in locations where the majority of the yearly precipitation occurs during one season. Variability in the magnitude of precipitation occurs on interannual time scales, for example, due to the El Niño–Southern Oscillation pattern, resulting in periods of higher or lower than normal precipitation for some regions [*Ropelewski and Halpert*, 1987]. Climate variability on centennial and millennial time scales in the Holocene resulted in changes in the frequency and magnitude of flood events in the American southwest [*Ely*, 1997]. Systematic climate variability during the Holocene on similar millennial time scales is also present in the central Rocky Mountains, resulting in higher flood magnitudes [*Carson et al.*, 2007] and episodes of lateral beveling and sediment aggradation followed by incision [*Pierce et al.*, 2011]. Thus, although the modeled storm-interstorm intervals substantially overstate the duration and timing of real storms, their mean values are compatible with seasonal variability and their extremes with interannual variability.

We allow the model to evolve into a condition of roughly uniform erosion over 5 M model years, after which we run model scenarios to investigate whether any of the suggested climatic drivers, either alone or in combination, results in strath terrace development and abandonment. The climate perturbations in the model are created using 782 kyr of a $\delta^{18}O$ curve [*Lisiecki and Raymo*, 2005], as a proxy for either glacial sediment flux, hillslope transport efficiency, or storm intensity. In each case, the variable in question is assumed to scale linearly with the isotopic value. We explore the terrace-forming potential of (1) sediment flux from a point source, (2) variations in hillslope transport efficiency, (3) variations in rainfall intensity, and (4) a combination of changes in both hillslope transport efficiency and rainfall intensity. We also use a control model run, in which hillslope diffusivity and storm intensity are held constant and there is no sediment input from a point source, in order to distinguish between fluctuations that arise from extrinsic model forcing and those that reflect internal variability in response to stochastic rainfall variation.

2.1. Variations in Glacial Sediment Flux

In the first model run, we vary sediment influx at a point on the upstream end of the model (Figure 2) to represent sediment sourced from a glacier in the headwaters of the model catchment. Sediment flux from the point representing the glacial outlet is controlled by setting the slope and drainage area of this point; the sediment flux at that point for each storm is then set equal to the carrying capacity, Q_c, of the flow at the sediment inlet. We set the drainage area of the inlet to 4000 m^2 and allowed the sediment flux to change by varying the slope between 0 and 0.74 following the $\delta^{18}O$ curve. We use this range of slopes so that the mean sediment flux during peak glacial intervals equals 1.5×10^5 m^3/yr. This value for sediment flux during peak glacial intervals in the model was determined from the area covered by glaciers during the last glacial maximum in the Boulder Creek watershed (147.6 km^2) multiplied by a maximum erosion rate in the area covered by glaciers (E_{gl}) of 1 mm/yr [*Ward et al.*, 2009] so that $Q_{sglacier}$ is 1.47×10^5 m^3/yr. The maximum erosion rate of 1 mm/yr is not likely to be long lived, but it is used as an upper bound for the sediment flux applied in this model.

2.2. Hillslope Diffusivity

In order to investigate the role played by variation in sediment influx from hillslopes in downstream aggradation and incision, we vary the efficiency of hillslope sediment flux by changing the hillslope diffusivity coefficient, K_d. Published values of K_d range from about 10^{-4} to 10^{-2} m^2/yr, with higher values of K_d associated with colder or wetter climates [*Oehm and Hallet*, 2005]. Numerical modeling of soil creep through frost heave shows that hillslope diffusivity ranges from 0 to 0.04 m^2/yr, with most efficient transport when mean annual temperature is −6°C [*Anderson et al.*, 2013]. K_d in the model run varies with climate following the $\delta^{18}O$ curve, with values ranging between 0 and 0.03 m^2/yr; K_d in the control run was held constant at 0.015 m^2/yr. The imposed changes in hillslope diffusivity could represent any number of climate-controlled processes that change the efficiency of sediment transport down hillslopes, including changes in vegetation cover [*Istanbulluoglu and Bras*, 2005], changes in permafrost and overland flow [*Bogaart et al.*, 2003], changes in temperature that cause faster or slower frost creep [*Delunel et al.*, 2010; *Anderson et al.*, 2013], or increased sediment transport from landsliding [*Fuller et al.*, 2009].

2.3. Rainfall Intensity

In the final model run, we prescribe changes in mean storm intensity so that lower intensity, longer-duration storms occur during glacial intervals and higher intensity, shorter-duration storms occur during interglacial intervals. Total average yearly rainfall remains the same throughout the model run. *Jarrett and Costa* [1983] showed that rainfall-dominated catchments have the potential for much higher peak flood discharge than snowmelt-dominated catchments. Currently, streams draining the Front Range have characteristics of both snowmelt-dominated and rainfall-dominated catchments and are susceptible to large peak flood discharges as a result of intense rain storms. With an increase in snow coverage during glacial intervals, these streams would tend to shift to more snowmelt-dominated catchments. *Carson et al.* [2007] used reconstructed cross-sectional areas of abandoned channels in the Uinta Mountains, to show that peak flood discharge varied by as much as 15–20% for much of the Holocene and that higher peak flood discharge coincided with warmer intervals during the Holocene. In order to represent such variations at the glacial-interglacial scale, we change the mean rainfall intensity from 10 m/yr (1.14 mm/h) as in the control run, to rainfall intensity that varies from a cold-period minimum of 5 m/yr (0.6 mm/h) to a warm-period maximum of 15 m/yr (1.7 mm/h).

3. Results

We employ four metrics in the models to determine whether the applied climate perturbations result in the formation of terrace surfaces similar to those that flank the Colorado Front Range: (1) episodes of stable or aggrading channel elevation, which presumably coincide with long periods of terrace surface occupation, (2) rapid channel incision and surface abandonment, (3) increased paleodenudation rates during terrace sediment deposition, and (4) broad flights of strath terraces along the modeled channels.

Because the model does not allow for lateral erosion, bedrock valleys do not develop during long periods when the channel is at equilibrium state. In the model, the only way for a wide bedrock valley to form is if the channel moves laterally by aggrading above the channel banks so that water is rerouted by avulsion on the landscape. The bedrock under the new channel position can then be vertically incised during large storms that clear the channel of sediment, even during periods when the channel is aggrading or covered in a thick layer of sediment. This contrasts with the conceptual model of strath terrace formation during long periods

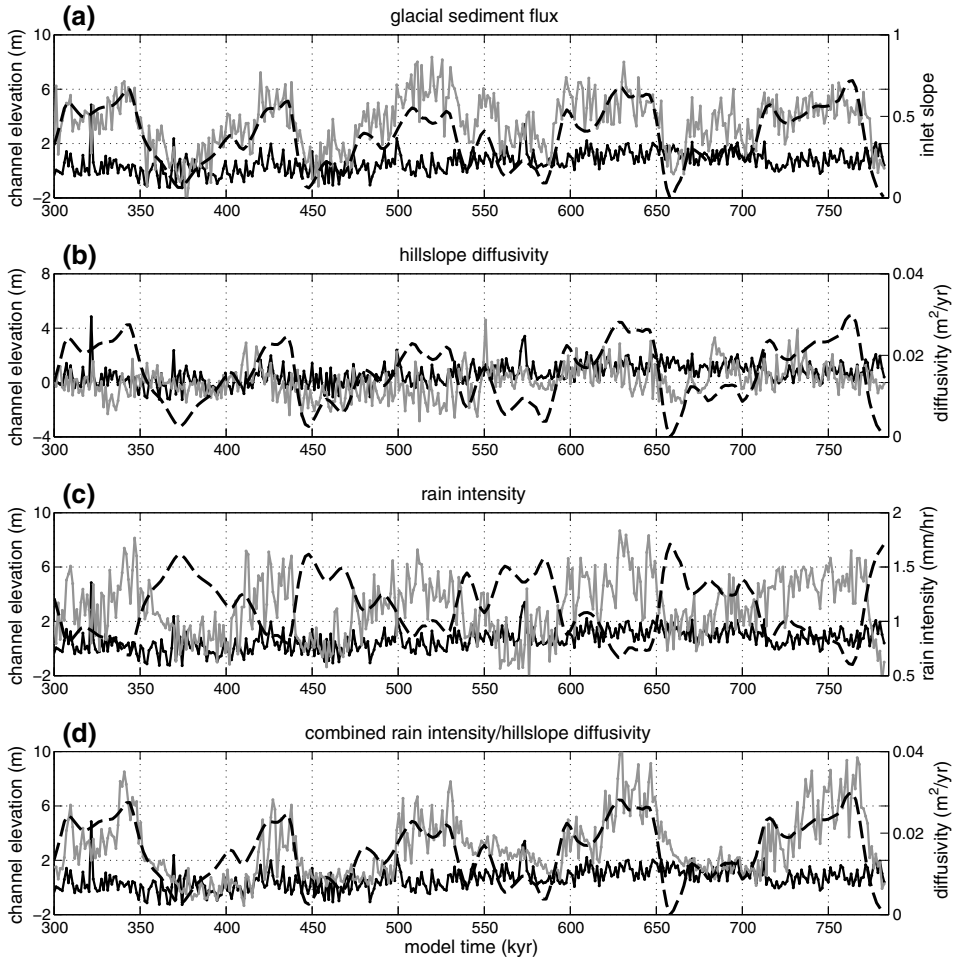

Figure 3. Mean elevation of the largest stream in the plains area of the model domain (Figure 2) for the model runs perturbed by climate changes (gray line) and the control model run (black line) divided by the beginning elevation of the control run. Dashed line shows climate forcing over the final 482 kyr of the model run. (a) Glacial sediment flux, (b) hillslope diffusivity, (c) rainfall intensity, and (d) combined rainfall intensity and hillslope diffusivity.

of channel equilibrium [*Bull*, 1990] but is supported by studies that demonstrate that deposition of sediment on the bed does not prevent a channel from eroding laterally to form a wide bedrock valley [*Hancock and Anderson*, 2002; *Johnson and Whipple*, 2010].

3.1. Variations in Glacial Sediment Flux

Adding a point that represents glacial sediment flux to the model results in cycles of aggradation and incision that smoothly follow changes to inlet slope, which is used as a proxy for sediment flux (Figure 3a). Figure 3a shows mean channel elevation on the plains for the control model run (black) and for the glacial sediment flux model run (gray). Here mean channel elevation refers specifically to the elevation of the largest stream that flows across the plains (Figure 2). Channel elevation in the control run fluctuates between 1.5 m below the starting value and 2 m above the starting value over the course of the 782 kyr model run. Many low-amplitude changes in sediment flux (such as from 450 to 500 kyr and 670 to 710 kyr in the model run) result in synchronous changes in channel elevation in the glacial sediment flux run, but the greatest magnitude sediment influx does not result in the greatest magnitude of channel aggradation. For example, from 460 to 560 kyr in the model run, sediment load rises, peaks, and declines. The peak sediment influx during this interval is not at the highest level during the model run, nor is higher sediment flux particularly long lasting during this interval. However, during this interval the channel aggrades to the highest level during the model run and its elevation remains relatively high.

The depth of interglacial intervals directly influences the magnitude of channel incision, while the magnitude of channel aggradation due to sediment flux from the inlet is controlled by both glacial stage, through the

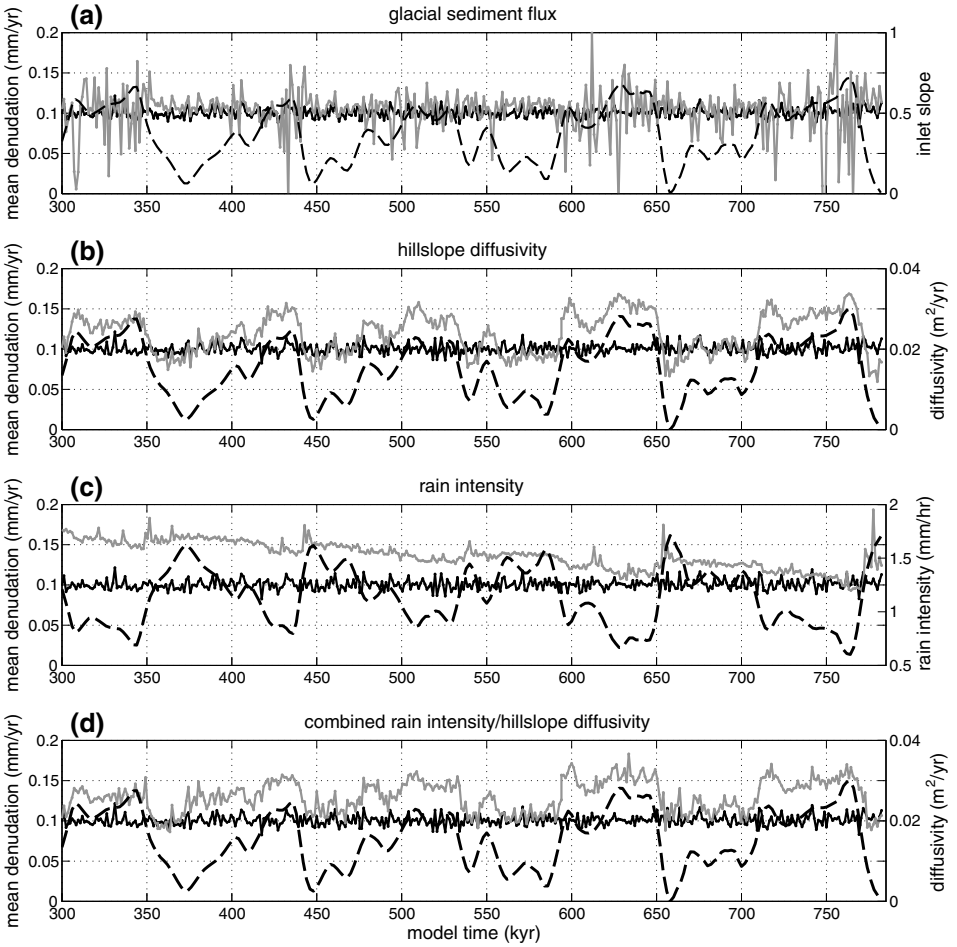

Figure 4. Mean denudation rates in the mountain area of the model domain for the model runs perturbed by climate changes (gray line) and the control model run (black line), along with the climate forcing (dashed line) over the final 482 kyr of the model run. The control model run is in a state of quasi-equilibrium and mean denudation rate in the mountains is steady at ~0.1 mm/yr, equal to the rate of uplift applied to the model. (a) Glacial sediment flux, (b) hillslope diffusivity, (c) rainfall intensity, and d) combined rainfall intensity-hillslope diffusivity.

slope of the inlet, and by the random duration and intensity of storms. During extended glacial intervals, the channel elevation shows up to 4 m of high-frequency variability over periods of a few thousand years. This pronounced variability in channel elevation only occurs when there is ample sediment supply; channel elevation is generally more steady during periods of incision.

Figure 4a shows the long-term rate of landscape lowering (i.e., denudation rate) averaged over the high-relief area of the model domain for the glacial sediment flux model and the control model. During periods of low and moderate sediment flux, denudation rates in the glacial sediment flux model are largely similar to denudation rates in the control run, about 0.1 mm/yr. During periods of high sediment flux, abrupt fluctuations in denudation rates in the mountains, ranging from 0 to 0.2 mm/yr, are an artifact of the model. These fluctuations are caused by sediment that fills the mountain channels, decreasing the slope between the channel and the hillslopes, slowing denudation from the hillslopes. The opposite occurs when mountain channels are flushed of sediment, resulting in a large pulse of rapid denudation. This effect is generally most pronounced near the sediment influx point.

Figure 5 shows cross sections of regolith and bedrock elevation across the model domain in the plains, 100 m beyond the edge of the mountains (Figure 2), for the glacial sediment flux run. Four different time steps are shown, demonstrating the effect of fluctuating glacial sediment flux on valley shape, channel aggradation, lateral movement of the channel, and bedrock planation by the channel. Figure 5a shows the glacial sediment flux model at 658 kyr into the model run, during a period of very low sediment flux. The bedrock valley is ~80 m

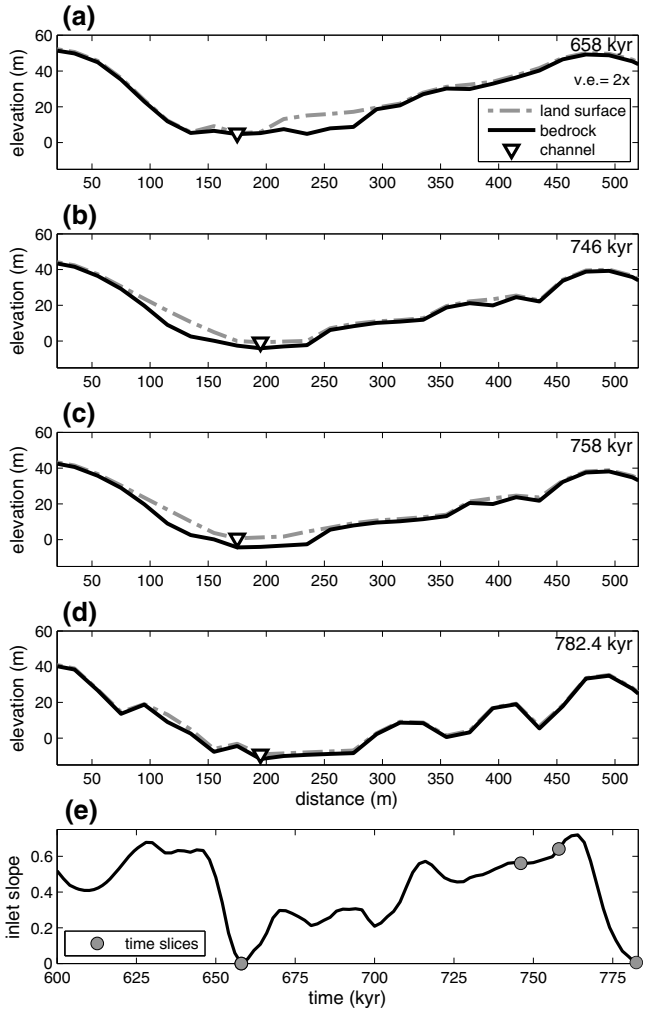

Figure 5. Cross sections at $y = 700$ m in model domain (Figure 2) for glacial sediment flux run at four different stages of sediment flux (Figures 5a–5d) and time series showing when model cross sections were taken (Figure 5e). Vertical exaggeration (v.e.) is 2 times. (a) During periods of very low sediment flux, the valley is wide, with negligible sediment cover. (b) Following an extended period of high sediment flux, the channel has shifted and the valley has filled with sediment. (c) At maximum sediment flux, the valley is filled with ~5 m of sediment. (d) Following rapid decrease in sediment flux, the valley is stripped of sediment and has widened by 30 m. (e) Time series showing inlet slope (a proxy for sediment flux in the model) for the last 180 kyr of the model run and when each cross section was taken.

wide with very little sediment coverage in the valley. The channel has incised into terrace fill that is ~10 m thick. After an extended period of high sediment flux, at 746 kyr, the valley has not widened significantly, but the channel has shifted slightly and there is a continuous cover of sediment on the valley floor (Figure 5b). At maximum sediment flux at 758 kyr, the bedrock valley is filled with ~5 m of sediment (Figure 5c). At 782.4 kyr, following a period of rapid sediment decrease over 18 kyr, the thick blanket of sediment in the bedrock valley has been stripped away and the bedrock valley has widened by about 30 m (Figure 5d).

3.2. Variations in Hillslope Transport Efficiency

Changing the efficiency of sediment transport on the hillslopes, K_d, from the control run value of 0.015 m^2/yr to values ranging between 0 and 0.03 m^2/yr has little net effect on aggradation and incision in the channel (Figure 3b). The channel has the potential to aggrade higher than the control model elevation during periods of high K_d and to incise during periods of low K_d (e.g., incision at 658 kyr, Figure 3b), but decreasing K_d does not always result in channel incision (e.g., little elevation change at 374 kyr, 564 kyr, and 586 kyr, Figure 3b). Increasing K_d tends to result in more variability in channel elevation during a cold period (500 kyr to 540 kyr model time) compared to a warm period (550 kyr to 590 kyr model time). There is no discernible lag between the forcing and channel response; if such lag is present, it is masked by the variability in the response signal.

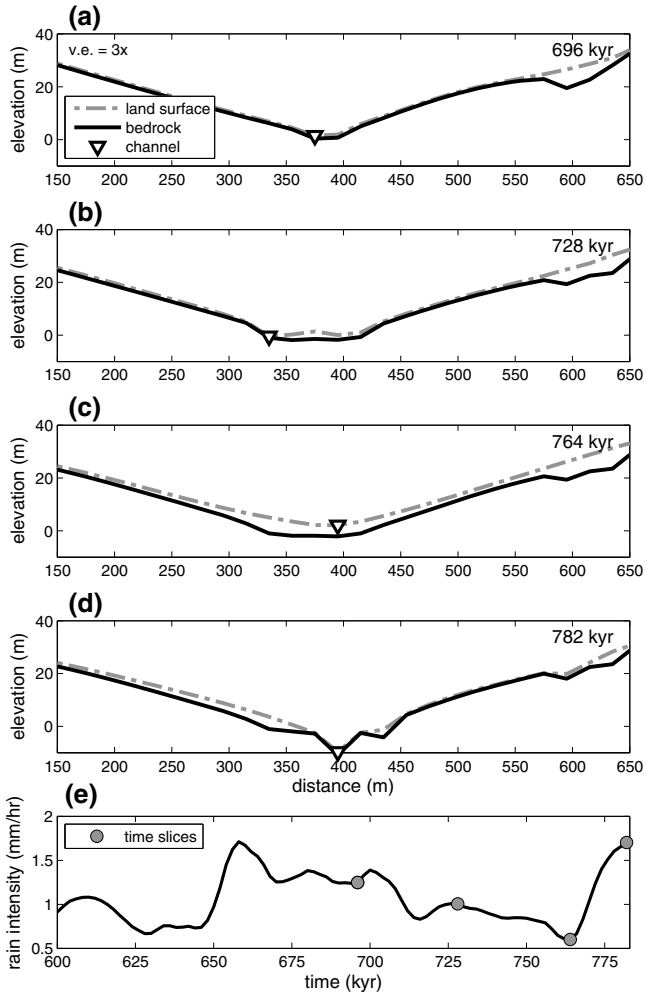

Figure 6. Cross sections at $y = 700$ m in model domain (Figure 2) for rainfall intensity run (Figures 6a–6d) and time series showing when model cross sections were taken (Figure 6e). Note that the landscape relief in the rainfall intensity run is much lower than the glacial sediment flux run and the combined rainfall intensity-hillslope diffusivity run. (a) During a high rainfall intensity period, the valley is narrow and V shaped, with little sediment cover. (b) Following a low rainfall intensity period, the valley has widened and the channel has shifted by 50 m. (c) During a period of very low rainfall intensity, the channel has shifted again by 60 m, and the valley is filled with ~4 m of sediment. (d) Following a sharp increase in rainfall intensity, the channel has incised vertically, leaving small, sediment-capped terraces 7 m above the channel. (e) Time series showing rainfall intensity for the last 180 kyr of the model run and when each cross section was taken.

Figure 4b shows mean denudation rate for the mountain area of the model domain for the model with variations in hillslope transport efficiency. Hillslope denudation rates follow the changes in K_d very smoothly and without a lag. Denudation rates are higher in this model run than in the control run due to the way that K_d is parameterized; mean hillslope diffusivity over the duration of the model run is 0.016 m^2/yr rather than 0.015 m^2/yr. During periods of high K_d, when sediment is transported very efficiently downslope, denudation rates increase from 0.1 mm/yr up to 0.17 mm/year. In order for denudation rates to fall below the long-term average, hillslope diffusivity must be very low, approaching 0; the lowest denudation rate for the model run is 0.05 mm/yr. In the final 20 kyr time interval of the model run, the mean denudation rate is nearly 3 times higher during the peak of the final glacial interval compared to the denudation rate during the final deep interglacial.

3.3. Variations in Rainfall Intensity

In the rainfall intensity model, we change mean rainfall intensity from the control run value of 1.14 mm/hr to mean rainfall intensity that varies from 0.57 mm/hr to 1.71 mm/hr, while adjusting the storm duration so that the average annual rainfall is the same for all runs. Note that the peak rainfall intensity from storm to storm

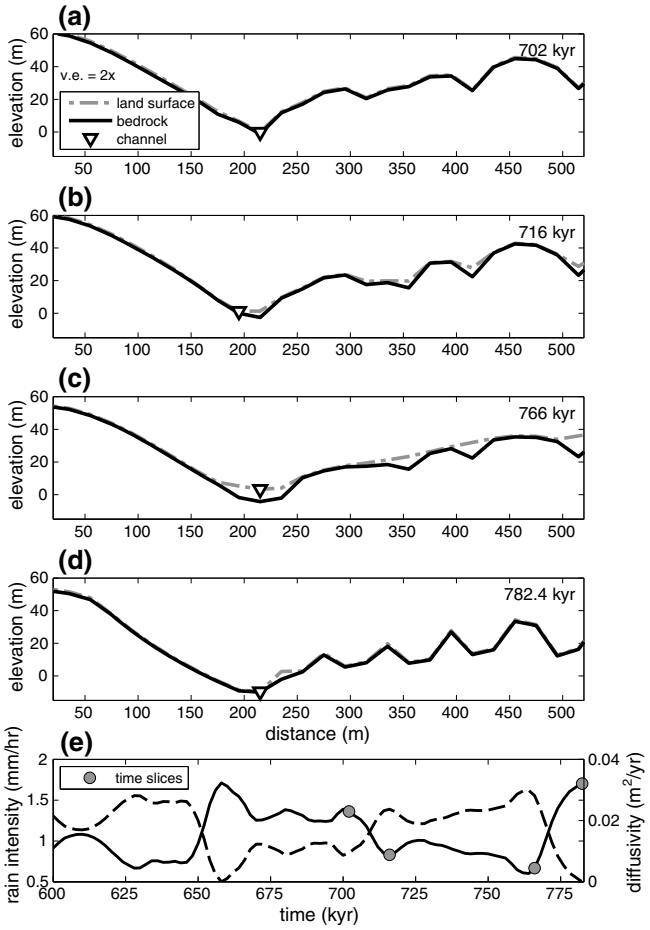

Figure 7. Cross sections at $y = 700$ m in model domain (Figure 2) for the combined rainfall intensity-hillslope diffusivity run (Figures 7a–7d) and time series showing when model cross sections were taken (Figure 7e). (a) During a period of high rainfall intensity and low hillslope diffusion, the valley is narrow and V shaped, with negligible sediment cover. (b) Following a shift to low rainfall intensity and higher hillslope diffusion, the channel has shifted and begun to erode the sides of the bedrock valley. (c) During an extended period of low rainfall intensity and high hillslope diffusion, the valley has widened by 80 m and is filled with ~7–8 m of sediment. (d) Following a sharp increase in rainfall intensity and decrease in hillslope diffusion, the channel has incised vertically through the sediment fill and bedrock, leaving a small, sediment-capped terrace above the channel. (e) Time series showing rainfall intensity (solid line) and hillslope diffusivity (dashed line) for the last 180 kyr of the model run and when each cross section was taken.

can be significantly higher than the mean. Periods of low mean rainfall intensity during glacial intervals result in the largest magnitude of channel aggradation seen in any of the model runs (Figure 3c). During periods of low mean rainfall intensity, the channel aggrades because there is less capacity to transport the sediment load. There is a threshold-like response in channel elevation to changes in rainfall intensity. For example, from 374 kyr to 402 kyr, rainfall intensity gradually decreases, but channel elevation remains low during the period. After rainfall intensity falls below ~1.25 mm/hr, the channel begins to aggrade. Channel incision commences again when mean rainfall intensity rises above ~1.25 mm/hr. The scale of channel aggradation is not very sensitive to the magnitude of the rainfall intensity, as long as it is below the threshold, nor does the magnitude of incision depend on the magnitude of rainfall intensity, as long as mean rainfall intensity is above the threshold. Channel elevation varies by as much as 5 m during periods of aggradation, as observed in other model runs.

Mean catchment-averaged denudation rates in the mountains for the rainfall intensity run are initially 3 times higher than the long-term average (Figure 4c), due to the increased rainfall intensity that rapidly denudes the landscape. By 750 kyr into the model run, mean denudation rates are nearly equal to the long-term average and the model has returned to a state such that erosion is equal to base level lowering. Despite the departure from the long-term average, it is apparent that during periods of low rainfall intensity, which correspond to

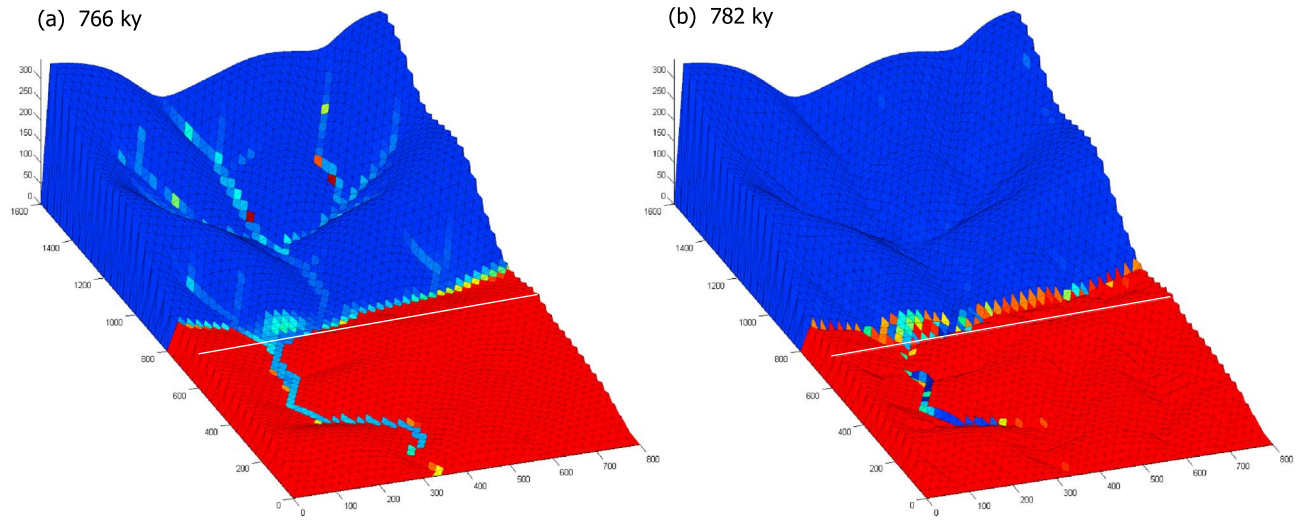

Figure 8. Model domain for two time points in the combined rainfall intensity-hillslope diffusivity run. The color overlay shows grain size distribution, with warm colors representing a high percentage of fine-grained material and the cool colors representing coarse-grained material. White line shows cross-section line in Figure 7. (a) Model domain at 766 kyr, during a period of low rainfall intensity-high diffusivity. The channel at $y = 700$ is 60 m wide (three model cells) and filled with coarse-grained sediment sourced from the mountains. (b) Model domain during period of high rainfall intensity-low diffusivity. Channel has incised into the fine-grained bedrock of the plains and is 10 m wide (one model cell).

glacial intervals, average denudation rates are lower than during interglacial intervals, which is contrary to evidence that paleodenudation rates were higher during glacial intervals when terrace-capping gravels were deposited [*Fuller et al.*, 2009; *Foster et al.*, 2013; *Dühnforth et al.*, 2012].

Figure 6 shows cross sections through the model domain at four different times, demonstrating the effect of changing rainfall intensity on valley shape, channel aggradation, lateral movement of the channel, and bedrock planation by the channel. Figure 6a shows the channel at 696 kyr into the model run, during a period of relatively high rainfall intensity. The valley is relatively narrow and V shaped and there is very little sediment covering the bottom of the channel. Figure 6b shows the channel at 728 kyr, during a period of low rainfall intensity. The valley has widened significantly and the channel has moved laterally by ~50 m. Much of the valley is blanketed in sediment, but during this interval the channel also occasionally bites down into the bedrock, forming a wide, flat valley bottom. At 764 kyr, during a period of very low mean rainfall intensity, the channel has moved again by 60 m and is completely filled with sediment (Figure 6c). Rainfall intensity increases sharply over the next 18 kyr, and by 782 kyr, the channel has incised vertically into the bedrock, forming a narrow, V-shaped valley leaving paired, sediment-capped terraces relatively high above the channel (Figure 6d).

3.4. Simultaneous Variations in Rainfall Intensity and Hillslope Transport Efficiency

In the final model run, we adjusted the climate with changes in both rainfall intensity and hillslope diffusivity. The opposing effects of lower hillslope diffusivity during periods with high rainfall intensity prevent excessive erosion and smoothing of the landscape compared to the rainfall intensity model (cf. Figures 6 and 7). Peaks in channel aggradation correlate with peaks in hillslope diffusivity, and general periods of high channel elevation correlate with extended periods of low rainfall intensity (Figures 3d and 7e). The periods of channel aggradation are shortened in the rainfall-diffusion model compared to the rainfall intensity model. The rainfall intensity threshold for aggradation is lower in the combined model, with aggradation only occurring when mean rainfall intensity falls below 1.1 mm/yr. The rainfall intensity-diffusion model has less variability during incisional periods than the rainfall intensity model run, but is equally variable in the aggradational periods.

The combined rainfall intensity-hillslope diffusion model run has long periods of elevated denudation rates during glacial periods, with the catchment-averaged denudation rate up to 1.9 times higher during glacial intervals than during interglacial intervals. Figure 4d shows average catchment-wide denudation rates in the mountains for the combined rainfall intensity-diffusion model run. Denudation rates for the combined model run smoothly follow changes in hillslope diffusivity, except when K_d is very low and rainfall intensity is very high. During these periods of low diffusivity and high rainfall intensity, denudation rates for the combined

run flatten out at or above the long-term average rate and do not fall below the long-term average, as in the hillslope transport efficiency run (Figures 4b and 4d). This is because during these periods, the higher rainfall intensity increases fluvial erosion, balancing the effect of very low or zero hillslope transport through diffusion.

Cross sections in the plains for four time steps in the combined rainfall intensity/hillslope diffusivity model show that during periods of high rainfall intensity and low hillslope diffusivity (representing interglacial periods), the channel is narrow and V shaped and there is negligible sediment in the channel (Figure 7a). Fourteen thousand years later in the model run, at 716 kyr, rainfall intensity has decreased, hillslope diffusivity has increased, and the channel has shifted and begun to erode the sides of the bedrock valley (Figure 7b). The bedrock valley walls in the model cannot be eroded laterally; in the model, the bedrock valley widens as the channel changes position through aggradation and avulsion, followed by renewed vertical incision in the new channel location. This process of channel aggradation, avulsion, and vertical bedrock incision results in effective bedrock planation and valley widening. Following 50 kyr of low rainfall intensity and high sediment flux from the hillslopes, by 766 kyr, the channel has widened the bedrock valley further to 80 m, and the valley is filled with sediment sourced from the mountains (Figure 7c), as shown by the coarse-grained sediment in the valleys (Figure 8a). Over the final 18 kyr of the model run, rainfall intensity increased while hillslope diffusivity decreased dramatically, resulting in vertical incision of the bedrock on the plains and the abandonment of one small sediment-capped terrace (Figures 7d and 8b).

4. Discussion

Three of the four models, glacial sediment flux, rainfall intensity, and combined rainfall intensity/hillslope diffusion, match the observation that periods of channel aggradation correspond to glacial intervals, while periods of vertical channel incision correspond with interglacial intervals. Only one of the model scenarios, the combined rainfall intensity/hillslope diffusion model, also shows increased denudation rates in the mountains during periods of aggradation, which is necessary to agree with observed higher paleodenudation rates during the deposition of terrace-capping sediment [*Fuller et al.*, 2009; *Foster et al.*, 2013; *Dühnforth et al.*, 2012].

The glacial sediment flux model has the appropriate pattern of long periods of channel aggradation and rapid channel incision (Figure 3a), but lacks a coherent signal of changes in denudation rates (Figure 4a). Although the glacial sediment flux model shows channel aggradation and incision associated with the formation of strath terraces, this model cannot explain strath terraces, along the western edge of the High Plains, that are present in small watersheds that were not significantly glaciated during the last glacial maximum, such as Coal Creek and Lefthand Creek. The presence of strath terraces in these catchments and other unglaciated catchments in the American West [e.g., *Hanson et al.*, 2006] calls for a climate-driven process that does not require direct input of sediment from glaciers [*Anderson et al.*, 2012]. Given that we model sediment supply from glaciers as a generic point source, any climate-driven point source of sediment may produce similar effects.

The hillslope diffusivity model does not show a coherent signal of aggradation and incision in the channels (Figure 3b), but does show denudation rates that are nearly three times higher during glacial intervals than during interglacial intervals (Figure 4b). Despite the increase in hillslope transport efficiency by a factor of three over the duration of the model run, the amount of sediment added to the stream is too small in relation to the transport capacity of the stream, Q_c, to cause significant channel aggradation. Aggradation and incision patterns in the detachment-limited channels of the hillslope diffusivity model are largely controlled by the variability in rainfall intensity and storm duration, allowing the channels to fill with sediment during quiescent periods and then rapidly flush the sediment out during intense storms.

The rainfall intensity model shows aggradation and incision in the channels (Figure 3c) resulting from changes in transport capacity, Q_c. The periods of intense rainfall during this model run reduced the relief of the landscape by vigorously eroding the hillslopes as well as incising the channels, while periods of low rain intensity resulted in channel migration and widening of the bedrock valley (Figure 6). The rainfall intensity model shows decreased denudation rates during glacial intervals, due to lower rainfall intensity and decreased erosion of hillslopes from running water (Figure 4c). Denudation rates are higher during interglacial periods due to intense rainfall, which efficiently strips the hillslopes of available sediment. Despite the increase in sediment flux in the channels during periods of intense rainfall, vertical incision still occurs because the increase in transport capacity is proportionately larger. This pattern of decreased denudation rates during glacial

intervals is the opposite of what is observed [*Fuller et al.*, 2009; *Foster et al.*, 2013; *Dühnforth et al.*, 2012], leading us to conclude that variation in rainfall intensity is not sufficient by itself to explain the genesis of the terraces flanking the Front Range. While the origin of the sediments analyzed by Foster and colleagues is not known with certainty, the fact that they occur on a surface that appears to have been formed by Lefthand Creek suggests that the material was eroded from the Lefthand Creek catchment some time during the last glacial period. If correct, it follows that the sediment does not derive from glacial erosion, because the Lefthand Creek catchment was not glaciated during the last glacial maximum. Within the crystalline Front Range, Lefthand Creek and its tributaries today occupy narrow bedrock valleys with little sediment storage. There is no evidence to suggest that these valleys held significant volumes of stored sediment before the last glacial period or that such sediment was evacuated during the glacial period. Thus, it seems reasonable to interpret the ^{10}Be concentration as primarily reflecting the denudation rate of hillslopes within the Lefthand Creek drainage basin during the last glacial period.

Combining the climate forcing mechanisms from the rainfall intensity model and the hillslope diffusivity model resolves the weaknesses of both models. The combined scenario matches three of the four markers of terrace development that we have identified: channel aggradation, channel incision, and increased denudation rates during terrace planation (Figures 3d and 4d). The combined rainfall intensity-hillslope diffusivity model can also explain the presence of strath terraces in catchments that have no evidence of past glaciation, such as Lefthand Creek and Coal Creek. The combined rainfall intensity-hillslope diffusivity model demonstrates that in the absence of a large influx of sediment, such as glacially sourced sediment, to a detachment-limited stream, the primary mechanism for channel aggradation is reducing the transport capacity of the stream.

Meyer et al. [1995] demonstrate the relationship between climate fluctuations in the Holocene and stream terrace genesis in another location in the American West, allowing us to compare our model results with a second field study, with the advantage of having several well dated terrace surfaces, local paleoclimate proxies, and modern analogies to the changing rainfall intensity and hillslope sediment supply. *Meyer et al.* [1995] link radiocarbon dates of Holocene fluvial terraces on alluvial streams in northwest Wyoming with paleoclimate records. They found that Holocene shifts in climate caused synchronous flood plain widening and overbank sedimentation, followed by channel incision in several streams in Yellowstone National Park. The model results presented here and the work of *Meyer et al.* [1995] both found that flood plains widen and terrace treads develop during cooler intervals, and surface abandonment and incision occurred during warmer intervals. *Meyer et al.* [1995] suggest flood plain widening occurring during cooler, wetter intervals when average discharge in the study streams is presumably larger than in warmer periods. The rainfall intensity model and combined rainfall intensity-hillslope diffusion model in this work also predict channel deposition and more lateral movement of the channel during glacial intervals, but in our models only average storm intensity and storm duration is changed, not average yearly rainfall. *Meyer et al.* [1995] suggest channel incision during warmer, more drought prone periods is caused by infrequent, channel bed scouring floods. We see a similar effect of channel incision in our model by applying more intense, longer duration storms to the model, but without decreasing average yearly rainfall.

4.1. Model Variability

We observe small, rapid variations around a long-term mean in channel elevation (Figure 3) and denudation rates (Figure 4) in all of the model runs, including the control run, which has no extrinsic forcing apart from stationary stochastic variability in rainfall input. We consider the variability we observe in the models on centennial to millennial timescales to be a reasonable representation of how natural systems operate. The dynamic fluctuation in the model between model output intervals (1200 years), requires us to observe patterns over several thousand years of the model runs to discern long-term trends. This becomes especially important during aggradational periods when the ratio of sediment load to carrying capacity is high and the magnitude of variability is amplified. The variability in channel elevation driven by random storms of varying size suggests that large storms that drastically increase carrying capacity can result in episodes of significant channel incision, even during intervals of net channel aggradation.

Terraces in the Lefthand Creek watershed suggest rapid incision during a glacial interval. Table Mountain and a lower adjacent terrace are offset by 20 vertical meters (Figure 1) and have very close reported abandonment ages [*Dühnforth et al.*, 2012; *Foster et al.*, 2013]. The amplified variability in channel elevation that we observe in the model as a result of large storms during aggradational periods provides an explanation for the apparently

rapid incision by Lefthand Creek at ~90–95 kyr, during a period that should generally have been characterized by high sediment load in the streams, strath terrace beveling, and fluvial sediment deposition.

4.2. Mechanisms for Bedrock Incision

Several authors [e.g., *Gilbert*, 1877; *Hancock and Anderson*, 2002] attribute the increase in the ratio of lateral to vertical erosion rates required to create strath terraces to armoring of the river bed due to increased sediment supply. Our models demonstrate this effect and show that widening of channel valleys and the creation of bedrock surfaces can occur due to episodic channel aggradation, avulsion, and punctuated bedrock incision. During periods of increased sediment flux or decreased stream transport, the model channels tend to fill with sediment, protecting the underlying bedrock from vertical incision (Figure 6c). The stochastic nature of the storms applied to the model means that even during periods when the channel bed is protected by overlying sediment cover, large storms can occur that expose the underlying bedrock to incision, and potentially, produce lateral bedrock valley widening (Figure 6b). Our models show that a bedrock strath can be generated without an explicit lateral erosion rule. During long periods of aggradation, an avulsion of the channel allows brief episodes of bed scour and vertical bedrock incision during large storm events. This concept of punctuated biting of the bedrock strath rather than continuous lateral planation of the bedrock may explain the undulating bedrock topography of the Rocky Flats surface [*Knepper*, 2005]; however, the lack of broad, drainage-spanning surfaces in the models suggests that this mechanism fails to explain fully the extensive strath terraces observed adjacent to the Front Range.

4.3. Model Limitations

A chief shortcoming of these models is their inability to create and preserve flights of terraces that are broad enough to span between adjacent drainage outlets and that extend up to the edge of the crystalline mountain front, as they do along the Front Range (Figure 1). The theory outlined in model description provides no mechanism for lateral erosion. In the numerical model, the only way for a stream to move laterally is for the stream bed to aggrade above the channel banks so that water is rerouted by avulsion on the landscape. We hypothesize that lateral channel erosion is the essential missing ingredient needed to form and preserve broad strath terraces like those that flank many Rocky Mountain ranges. CHILD, like most other landscape evolution models, does not include a mechanism for lateral erosion of the bedrock channel, although there are several generations of landscape evolution models that capture meandering in alluvial rivers [e.g., *Lancaster and Bras*, 2002; *Coulthard and van de Wiel*, 2006] and models that take adjustments in channel width into account [*Turowski et al.*, 2008; *Yanites and Tucker*, 2010]. So far the only landscape evolution model that attempts to capture lateral bedrock erosion is the 1-D model of *Hancock and Anderson* [2002], which does so through an ad hoc lateral erosion rule based on stream power and ratio of channel width to total valley width in order to explain the observation that beveling a bedrock strath requires much higher rates of lateral planation compared to vertical incision. Understanding the processes critical to lateral erosion and implementing them into landscape evolution theory and computational model remains a frontier in geomorphology [*Lague*, 2010].

5. Conclusions

Three of the four model scenarios driven by different climate forcings show vertical bedrock incision during periods of low sediment flux or intense rainfall and aggradation during the opposite phases of a climate cycle. Increasing hillslope diffusivity by a factor of 4 did not produce cyclic aggradation and incision, because the amount of sediment added to the rivers was too small in comparison with the carrying capacity of the stream. Only the hillslope diffusivity model and the combined rainfall intensity-hillslope diffusivity models produced higher erosion rates in the mountains during glacial intervals, leading us to conclude that processes that increase hillslope sediment flux must play a role in increasing the sediment load that both promotes lateral valley widening and deposition of sediment on terraces during glacial intervals. An alternate explanation that increased sediment flux during glacial intervals is the result of changes in rainfall intensity and duration and appears to be insufficient to produce both channel aggradation and increased paleodenudation rates. In nature, the unusual breadth of the strath terraces that flank the Front Range arises from efficient lateral erosion on easily eroded rocks of the High Plains. None of the model scenarios produced flights of broad strath terraces, suggesting that an explicit lateral bedrock erosion rule is indeed required to explain the remarkable breadth of these range-bounding terraces.

Acknowledgments
This work was funded by NSF grant EAR-0724960. Data for this paper can be accessed from http://criticalzone.org/boulder/data/datasets/ or by e-mailing A. Langston. The CHILD model can be downloaded from http://csdms.colorado.edu/wiki/Model:CHILD, doi: 10.1594/IEDA/100102. This work was funded by NSF grant EAR-0724960. Thanks go to Melissa Foster for many insightful discussions about terrace genesis and two reviewers whose comments greatly improved this manuscript.

References

Anderson, R. S., S. P. Anderson, and G. E. Tucker (2013), Rock damage and regolith transport by frost: An example of climate modulation of the geomorphology of the critical zone, *Earth Surf. Processes Landforms*, *38*, 299–316.

Anderson, S. P., R. S. Anderson, and G. E. Tucker (2012), Landscape scale linkages in critical zone evolution, *C. R. Geosci.*, *344*(11–12), 586–596.

Bogaart, P. W., G. E. Tucker, and J. De Vries (2003), Channel network morphology and sediment dynamics under alternating periglacial and temperate regimes: A numerical simulation study, *Geomorphology*, *54*(3), 257–277.

Brocard, G. Y., and P. A. Van der Beek (2006), Influence of incision rate, rock strength, and bedload supply on bedrock river gradients and valley-flat widths: Field-based evidence and calibrations from western Alpine rivers (southeast France), *Geol. Soc. Spec. Pap.*, *398*, 101–126.

Brocard, G. Y., P. A. Van Der Beek, D. Bourlès, and J.-L. Siame (2003), Long-term fluvial incision rates and postglacial river relaxation time in the French Western Alps from ^{10}Be dating of alluvial terraces with assessment of inheritance, soil development and wind ablation effects, *Earth Planet. Sci. Lett.*, *209*(1), 197–214.

Bull, W. B. (1979), Threshold of critical power in streams, *Geol. Soc. Am. Bull.*, *90*(5), 453–464.

Bull, W. B. (1990), Stream-terrace genesis: Implications for soil development, *Geomorphology*, *3*(3), 351–367.

Carson, E. C., J. C. Knox, and D. M. Mickelson (2007), Response of bankfull flood magnitudes to holocene climate change, Uinta Mountains, northeastern Utah, *Geol. Soc. Am. Bull.*, *119*(9–10), 1066–1078.

Church, M., and O. Slaymaker (1989), Disequilibrium of Holocene sediment yield in glaciated British Columbia, *Nature*, *337*(6206), 452–454.

Coulthard, T., and M. J. van de Wiel (2006), A cellular model of river meandering, *Earth Surf. Processes Landforms*, *31*(1), 123–132.

Delunel, R., P. A. Van Der Beek, J. Carcaillet, D. L. Bourlès, and P. G. Valla (2010), Frost-cracking control on catchment denudation rates: Insights from in situ produced ^{10}Be concentrations in stream sediments (Ecrins–Pelvoux massif, French Western Alps), *Earth Planet. Sci. Lett.*, *293*(1), 72–83.

Dethier, D., and E. Lazarus (2006), Geomorphic inferences from regolith thickness, chemical denudation and CRN erosion rates near the glacial limit, Boulder Creek catchment and vicinity, Colorado, *Geomorphology*, *75*(3–4), 384–399.

DeVecchio, D. E., R. V. Heermance, M. Fuchs, and L. A. Owen (2012), Climate-controlled landscape evolution in the Western Transverse Ranges, California: Insights from Quaternary geochronology of the Saugus Formation and strath terrace flights, *Lithosphere*, *4*(2), 110–130.

Dühnforth, M., R. S. Anderson, D. J. Ward, and A. Blum (2012), Unsteady late Pleistocene incision of streams bounding the Colorado Front Range from measurements of meteoric and in situ ^{10}Be, *J. Geophys. Res.*, *117*, F01023, doi:10.1029/2011JF002232.

Eagleson, P. S. (1978), Climate, soil, and vegetation: 2. The distribution of annual precipitation derived from observed storm sequences, *Water Resour. Res.*, *14*(5), 713–721.

Ely, L. L. (1997), Response of extreme floods in the southwestern United States to climatic variations in the late Holocene, *Geomorphology*, *19*(3), 175–201.

Finnegan, N. J., and G. Balco (2013), Sediment supply, base level, braiding, and bedrock river terrace formation: Arroyo Seco, California, USA, *Geol. Soc. Am. Bull.*, *125*(7–8), 1114–1124.

Finnegan, N. J., and W. E. Dietrich (2011), Episodic bedrock strath terrace formation due to meander migration and cutoff, *Geology*, *39*(2), 143–146.

Foster, M. A., M. Duhnforth, and R. S. Anderson (2013), Strath terraces on the western High Plains indicate climatically-driven variations in sediment supply from source basins in the Colorado Front Range, Abstract EP23B-08 presented at 2013 Fall Meeting, AGU, San Francisco, Calif., 9–13 Dec.

Fuller, T. K., L. A. Perg, J. K. Willenbring, and K. Lepper (2009), Field evidence for climate-driven changes in sediment supply leading to strath terrace formation, *Geology*, *37*(5), 467–470.

Gasparini, N. M., G. E. Tucker, and R. L. Bras (1999), Downstream fining through selective particle sorting in an equilibrium drainage network, *Geology*, *27*(12), 1079–1082.

Gilbert, G. K. (1877), *Report on the Geology of the Henry Mountains*, p. 170, U.S. Gov. Print. Off., Washington, D. C.

Hancock, G. S., and R. S. Anderson (2002), Numerical modeling of fluvial strath-terrace formation in response to oscillating climate, *Geol. Soc. Am. Bull.*, *114*, 1131–1142.

Hancock, G. S., R. S. Anderson, O. A. Chadwick, and R. C. Finkel (1999), Dating fluvial terraces with ^{10}Be and ^{26}Al profiles: Application to the Wind River, Wyoming, *Geomorphology*, *27*(1), 41–60.

Hanson, P. R., J. A. Mason, and R. J. Goble (2006), Fluvial terrace formation along Wyoming's Laramie Range as a response to increased late Pleistocene flood magnitudes, *Geomorphology*, *76*(1), 12–25.

Heimsath, A. M., W. E. Dietrich, K. Nishiizumi, and R. C. Finkel (1997), The soil production function and landscape equilibrium, *Nature*, *388*(6640), 358–361.

Istanbulluoglu, E., and R. L. Bras (2005), Vegetation-modulated landscape evolution: Effects of vegetation on landscape processes, drainage density, and topography, *J. Geophys. Res.*, *110*, F02012, doi:10.1029/2004JF000249.

Jarrett, R. D., and J. E. Costa (1983), Multidisciplinary approach to the flood hydrology of foothill streams in Colorado, in *International Symposium on Hydrometeorology June 13–17, 1982, Denver, Colorado*, edited by A. I. Johnson and R. A. Clark, pp. 565–569, Am. Water Res. Assoc., Bethesda, Md.

Johnson, J. P., and K. X. Whipple (2010), Evaluating the controls of shear stress, sediment supply, alluvial cover, and channel morphology on experimental bedrock incision rate, *J. Geophys. Res.*, *115*, F02018, doi:10.1029/2009JF001335.

Knepper, D. H. (2005), Bedrock erosion surface beneath the Rocky Flats alluvial fan, Jefferson and Boulder counties, Colorado, *Mt. Geol.*, *42*, 1–10.

Lague, D. (2010), Reduction of long-term bedrock incision efficiency by short-term alluvial cover intermittency, *J. Geophys. Res.*, *115*, F02011, doi:10.1029/2008JF001210.

Lancaster, S. T., and R. L. Bras (2002), A simple model of river meandering and its comparison to natural channels, *Hydrol. Processes*, *16*(1), 1–26.

Lisiecki, L. E., and M. E. Raymo (2005), A Pliocene-Pleistocene stack of 57 globally distributed benthic δ^{18}O records, *Paleoceanography*, *20*, PA1003, doi:10.1029/2004PA001071.

Madole, R. F. (1991), Quaternary geology of the northern Great Plains, Colorado Piedmont section, in *Quaternary Nonglacial Geology; Conterminous United States*, vol. 2, edited by R. B. Morrison, pp. 456–462, Geol. Soc. Am., Boulder, Colo.

Madole, R. F., D. P. VanSistine, and J. Michael (1998), *Pleistocene Glaciation in the Upper Platte River Drainage Basin, Colorado, U.S. Geol. Surv. 2644*, IMAP, Boulder, Colo.

Merritts, D. J., K. R. Vincent, and E. E. Wohl (1994), Long river profiles, tectonism, and eustasy: A guide to interpreting fluvial terraces, *J. Geophys. Res.*, *99*(B7), 14,031–14,050.
Meyer, G. A., S. G. Wells, and A. T. Jull (1995), Fire and alluvial chronology in Yellowstone National Park: Climatic and intrinsic controls on Holocene geomorphic processes, *Geol. Soc. Am. Bull.*, *107*(10), 1211–1230.
Molnar, P., et al. (1994), Quaternary climate-change and the formation of river terraces across growing anticlines on the north flank of the Tien-Shan, China, *J. Geol.*, *102*, 583–602.
Montgomery, D. R. (2004), Observations on the role of lithology in strath terrace formation and bedrock channel width, *Am. J. Sci.*, *304*(5), 454–476.
Oehm, B., and B. Hallet (2005), Rates of soil creep, worldwide: Weak climatic controls and potential feedback, *Z. Geomorphol.*, *49*(3), 353–372.
Pan, B., D. Burbank, Y. Wang, G. Wu, J. Li, and Q. Guan (2003), A 900 k.y. record of strath terrace formation during glacial-interglacial transitions in northwest China, *Geology*, *31*(11), 957–960.
Pierce, J. L., G. A. Meyer, and T. Rittenour (2011), The relation of Holocene fluvial terraces to changes in climate and sediment supply, South Fork Payette River, Idaho, *Quat. Sci. Rev.*, *30*(5), 628–645.
Riihimaki, C. A., R. S. Anderson, E. B. Safran, D. P. Dethier, R. C. Finkel, and P. R. Bierman (2006), Longevity and progressive abandonment of the Rocky Flats surface, Front Range, Colorado, *Geomorphology*, *78*(3), 265–278.
Ropelewski, C. F., and M. S. Halpert (1987), Global and regional scale precipitation patterns associated with the El Niño/Southern Oscillation, *Mon. Weather Rev.*, *115*(8), 1606–1626.
Schildgen, T., D. Dethier, P. Bierman, and M. Caffee (2002), ^{26}Al and ^{10}Be dating of late Pleistocene and Holocene fill terraces: A record of fluvial deposition and incision, Colorado Front Range, *Earth Surf. Processes Landforms*, *27*(7), 773–787.
Tucker, G. E. (2004), Drainage basin sensitivity to tectonic and climatic forcing: Implications of a stochastic model for the role of entrainment and erosion thresholds, *Earth Surf. Processes Landforms*, *29*(2), 185–205.
Tucker, G. E., and R. L. Bras (2000), A stochastic approach to modeling the role of rainfall variability in drainage basin evolution, *Water Resour. Res.*, *36*(7), 1953–1964.
Tucker, G. E., and G. R. Hancock (2010), Modelling landscape evolution, *Earth Surf. Processes Landforms*, *35*(1), 28–50.
Tucker, G. E., and R. L. Slingerland (1997), Drainage basin response to climate change, *Water Resour. Res.*, *33*, 2031–2047.
Tucker, G. E., S. T. Lancaster, N. M. Gasparini, and R. L. Bras (2001), The Channel-Hillslope Integrated Landscape Development Model (CHILD), in *Landscape Erosion and Evolution Modeling*, edited by R. S. Harmon and W. W. Doe, pp. 349–388, Kluwer Press, Dordrecht.
Turowski, J. M., N. Hovius, H. Meng-Long, D. Lague, and C. Men-Chiang (2008), Distribution of erosion across bedrock channels, *Earth Surf. Processes Landforms*, *33*(3), 353–363.
Vandenberghe, J. (2003), Climate forcing of fluvial system development: An evolution of ideas, *Quat. Sci. Rev.*, *22*(20), 2053–2060.
Ward, D. J., R. S. Anderson, Z. S. Guido, and J. P. Briner (2009), Numerical modeling of cosmogenic deglaciation records, Front Range and San Juan Mountains, Colorado, *J. Geophys. Res.*, *114*, F01026, doi:10.1029/2008JF001057.
Wegmann, K. W., and F. J. Pazzaglia (2002), Holocene strath terraces, climate change, and active tectonics: The Clearwater River basin, Olympic Peninsula, Washington State, *Geol. Soc. Am. Bull.*, *114*(6), 731–744.
Whipple, K. X., G. S. Hancock, and R. S. Anderson (2000), River incision into bedrock: Mechanics and relative efficacy of plucking, abrasion, and cavitation, *Geol. Soc. Am. Bull.*, *112*(3), 490–503.
Yanites, B. J., and G. E. Tucker (2010), Controls and limits on bedrock channel geometry, *J. Geophys. Res.*, *115*, F04019, doi:10.1029/2009JF001601.